Available online at www.sciencedirect.com
SCIENCE DIRECT
Journal of Catalysis 228 (2004) 374–385
JOURNAL OF CATALYSIS
www.elsevier.com/locate/jcat

Preparation of microporous acidic oxides from aluminum-bridged silsesquioxanes and catalytic activities for the cracking of hydrocarbons

Kenji Wada *, Kiyohiko Tada, Naohiko Itayama, Teruyuki Kondo, Take-aki Mitsudo *

Department of Energy and Hydrocarbon Chemistry, Graduate School of Engineering, Kyoto University, Nishikyo-ku, Kyoto 615-8510, Japan

Received 31 May 2004; revised 2 September 2004; accepted 6 September 2004

Abstract

The catalytic activities of a series of porous oxides prepared from silsesquioxanes for the cracking of hydrocarbons have been examined. In addition to known group 13 element-containing silsesquioxanes, new aluminum-bridged silsesquioxanes bearing various countercations, $[Y]^+[\{(c\text{-}C_5H_9)_7Si_7O_{12}(SiMe_3)\}_2Al]^-$ ($[Y]^+ = [H_2NMe_2]^+$ (**2b**), $[HNMe_2(C_8H_{17})]^+$ (**2c**), $[HNMe_2(C_{18}H_{37})]^+$ (**2e**), $[HNC_5H_5]^+[\{(c\text{-}C_5H_9)_8Si_8O_{13}\}_2Al]^-$ (**3d**), and $[HNC_5H_5]^+[\{(i\text{-}C_4H_9)_8Si_8O_{13}\}_2Al]^-$ (**4d**), have been synthesized. The controlled calcination of these silsesquioxanes at around 823 K produced amorphous porous acidic oxides with high BET surface areas of 360–520 $m^2\,g^{-1}$ and uniformly controlled micropores of 5–6 Å diameter. Among the oxides examined, those prepared from aluminum-bridged silsesquioxanes show excellent catalytic activities for the cracking of cumene even at low reaction temperatures of around 523 K. Under identical conditions commercially available silica–alumina catalysts do not show significant activities, indicating exceptionally high activities of the silsesquioxane-based oxides despite their amorphous nature.

Keywords: Aluminum; Silsesquioxane; Microporous oxides; Solid acidic catalysts; Cracking of cumene

1. Introduction

The preparation of aluminosilicates of varying acidic properties and pore structures has been extensively studied because of their great importance in the chemical industry and petroleum refineries mainly as solid acidic catalysts [1,2]. The development of novel solid oxide materials with controlled acidic character and well-defined pores is especially of great significance.

Also, metal-containing oligosilsesquioxanes with cubic core structures have attracted attention as well-defined, homogeneous models for the active surface sites of the supported catalysts or metal-containing zeolites [3–10]. Several silsesquioxanes containing gallium [11,18], aluminum [12–18], or boron [18–20] have also been synthesized. In addition to their use as *homogeneous* catalysts, silsesquioxanes have been utilized as precursors of *heterogeneous* catalysts with novel properties and functionalities [21–36]. For example, we have reported excellent activities of the oxide catalysts prepared from a silica-supported vanadium-containing silsesquioxane for selective photo-assisted oxidation of methane into methanal [25]. The resulting oxide catalysts possessed markedly larger specific surface areas than those of the parent silica supports. In addition, for the first time we found that a metal-containing silsesquioxane can be a convenient precursor for M–Si–O materials with high surface areas and uniformly controlled micropores [26]. The following studies by us and others demonstrate the high utility of this method for the preparation of microporous oxides of various compositions [27–34]. Recently, we have found that the controlled calcination of several group 13 element-containing silsesquioxanes at around 823 K produces Brønsted acidic oxides with high BET surface areas of 360–520 $m^2\,g^{-1}$ and uniformly controlled micropores of 5.1 Å diameter [28,29], but examination of their catalytic ac-

* Corresponding authors. Fax: +81-75-383-2510.
E-mail addresses: wadaken@scl.kyoto-u.ac.jp (K. Wada), mitsudo@scl.kyoto-u.ac.jp (T.-a. Mitsudo).

0021-9517/$ – see front matter
doi:10.1016/j.jcat.2004.09.009

tivities is not included. However, Maxim et al. reported that the calcination of Brønsted acidic aluminosilsesquioxane, $[H]^+[\{(c\text{-}C_5H_9)_7Si_7O_{12}(SiMe_3)\}_2Al]^-$ (**2g**), resulted in the formation of Lewis acidic microporous oxides [32]. In this report the properties of the oxides as well as the effect of calcination conditions were thoroughly investigated by means of various spectroscopic methods, but their catalytic activities were only briefly examined. They test the activities of oxides toward the reaction of 1-butanol and found that at 200 °C dehydration to 1-butene was predominant, whereas the cracking reaction became predominant at 300 °C. Obviously, the evaluation and fine tuning of the catalytic properties of the oxides prepared from group 13 element-containing silsesquioxane toward the cracking of hydrocarbons are of great importance.

In the present paper, we have extended our previous work [28,29] to the preparation of acidic oxides from a number of group 13 element-containing molecules, mainly aluminum-bridged silsesquioxanes bearing various countercations or organic substituents and the examination their catalytic activities toward the cracking of model hydrocarbons, mainly cumene. Included this report is the synthesis of several new aluminum-containing silsesquioxane derivatives. A detailed characterization of the oxide catalysts is also reported.

2. Experimental

2.1. Materials

Trimethylaluminum in hexane solution (1 M), $(c\text{-}C_5H_9)_7Si_7O_9(OH)_3$, $(c\text{-}C_5H_9)_7Si_8O_{11}(OH)_2$, $(i\text{-}C_4H_9)_7Si_8O_{11}(OH)_2$, and $(t\text{-}C_4H_9O)_3SiOH$ were purchased from Aldrich and used as received. Organic solvents such as hexane, benzene, toluene, tetrahydrofurane (THF), diethyl ether, and triethylamine were carefully distilled using appropriate drying reagents just before use [37]. Other organic reagents were delivered from Wako Chemicals Co., Ltd., and Nacarai Tesque and used without further purification. Silsesquioxane disilanols, $(c\text{-}C_5H_9)_7Si_7O_{10}(RSiMe_2)(OH)_2$ (R = Me, allyl), were prepared by the kinetically controlled monosilylation of $(c\text{-}C_5H_9)_7Si_7O_9(OH)_3$ [38,39]. The detailed synthetic procedure of boron- and gallium-containing silsesquioxanes **1**, **6a**, and **6b** was reported elsewhere [28,29]. Aluminum-bridged silsesquioxanes **2a** [15,16], **2d**, and **2g** [16] were prepared according to known literature procedures. The reference catalysts, JRC-Z5-90H(1) and amorphous aluminosilicates (CCIC-LA), were provided by the Catalysis Society of Japan and Shokubai Kasei Kogyo Co.Ltd., respectively.

2.1.1. Synthesis of $[Y]^+[\{(c\text{-}C_5H_9)_7Si_7O_{12}(SiMe_2R)\}_2Al]^-$ (2b–f)

All synthetic procedures were carried out under an argon atmosphere by standard Schlenk techniques. Silsesquioxanes **2b–f** were prepared by the modified method reported for $[HNEt_3]^+[\{(c\text{-}C_5H_9)_7Si_7O_{12}(SiMe_3)\}_2Al]^-$ (**2a**) [16]. To a hexane solution (70 cm^3) of silsesquioxane disilanol, $(c\text{-}C_5H_9)_7Si_7O_{10}(RSiMe_2)(OH)_2$ (R = Me, allyl, 2.0 mmol) was added dropwise to a hexane solution (1.0 cm^3) of triethylaluminum (1 M, 1.0 mmol) at 0 °C. Amine (1.2 mmol) was added at 0 °C, followed by stirring at room temperature for 20 h. After removal of the solvent, recrystallization by slow diffusion of acetone into the toluene solution afforded colorless crystals of the desired aluminum-bridged silsesquioxanes with the corresponding ammonium cations in moderate yields.

2.1.1.1. ***2b*** *($[Y]^+ = [H_2NEt_2]^+$, R = Me).* Yield 53%. ^{1}H NMR (400 MHz, $CDCl_3$, 25 °C) δ8.27 (br s, 2H, $[H_2NEt_2]^+$), 3.27–3.00 (br m, 4H, $[H_2N(CH_2CH_3)_2]^+$), 1.71–1.24 (br m, 118H, CH_2 of Cy, $[H_2N(CH_2CH_3)_2]^+$), 0.94–0.76 (br m, 14H, C*H* of Cy), 0.10 (s, 18H, Si*Me*$_3$); ^{13}C NMR (100 MHz, $CDCl_3$, 25 °C) δ 39.50 (br, $[H_2N(CH_2CH_3)_2]^+$), 28.23, 28.17, 28.16, 28.01, 27.85, 27.73, 27.70, 27.62, 27.55, 27.44, 27.27, 27.21, 27.20, 27.17, 27.07, 27.03, 26.99, 26.94, 26.92, 26.90 (CH_2 of Cy), 25.07, 24.59, 24.20, 23.73, 22.83, 22.61 (*ipso-C*H of Cy), 1.83 (Si*Me*$_3$); ^{29}Si NMR (76 MHz, $CDCl_3$, 0.02 M $Cr(acac)_3$, 25 °C) δ 8.48, −64.42, −64.49, −64.96, −65.43, −67.53, −67.83. Anal. Calcd for $C_{80}H_{156}O_{24}NSi_{16}Al$ (1992.46): C, 48.23; H, 7.89; N, 0.70%. Found C, 47.83; H, 7.46; N, 0.68%.

2.1.1.2. ***2c*** *($[Y]^+ = [HNMe_2(n\text{-octyl})]^+$, R = Me).* Yield 31%. ^{1}H NMR (400 MHz, $CDCl_3$, 25 °C) δ 10.65 (br, 1H, $[HNMe_2(n\text{-octyl})]^+$), 3.15 (br m, 2H, $[HNMe_2(CH_2(CH_2)_6CH_3)]^+$), 2.88 (br m, 6H, $[HNMe_2(n\text{-octyl})]^+$), 2.36–1.50 (br m, 124H, CH_2 of Cy and $[HNMe_2(n\text{-octyl})]^+$), 1.50–1.11 (br m, 17H, *ipso*-C*H* of Cy, $[HNMe_2(CH_2)_{17}CH_3]^+$), 0.10 (s, 18H, Si*Me*$_3$); ^{13}C NMR (100 MHz, $CDCl_3$, 25 °C) δ 56.42, 31.74, 29.50, 29.32, 22.72, 21.90 ($[HNMe_2(CH_2)_7CH_3]^+$), 42.26, 42.16 ($[HNMe_2(n\text{-octyl})]^+$), 28.26, 28.20, 28.15, 28.05, 28.02, 27.87, 27.72, 27.67, 27.56, 27.44, 27.36, 27.30, 27.25, 27.21, 27.16, 27.06, 27.03, 26.95, 26.93, 26.89 (CH_2 of Cy and $[HNMe_2(n\text{-octyl})]^+$), 25.22, 25.19, 24.81, 24.16, 23.79, 22.84, 22.61 (*ipso-C*H of Cy), 14.12 ($[HN(CH_3)_2(CH_2)_7CH_3]^+$), 2.23 ($Si(CH_3)_3$); ^{29}Si NMR (76 MHz, $CDCl_3$, 0.02 M $Cr(acac)_3$, 25 °C) δ 8.08, −64.54, −64.69, −65.08, −65.26, −65.53, −67.95, −68.17. Anal. Calcd for $C_{86}H_{168}O_{24}Si_{16}AlN$ (2076.60): C, 49.74; H, 8.15; N, 0.67%. Found C, 49.68; H, 8.15; N, 0.60%.

2.1.1.3. ***2e*** *($[Y]^+ = [HNMe_2(n\text{-octadecyl})]^+$, R = Me).* Yield 97%. ^{1}H NMR (400 MHz, $CDCl_3$, 25 °C) δ 10.62 (br s, 1H, $[HNMe_2(n\text{-octadecyl})]^+$), 3.08 (br m, 2H, $[HNMe_2(CH_2(CH_2)_{16}CH_3)]^+$), 2.87 (br m, 6H, $[HNMe_2(n\text{-octadecyl})]^+$), 1.69–1.24 (br m, 144H, CH_2 of Cy and $[HNMe_2(n\text{-octadecyl})]^+$), 0.90–0.71 (br m, 17H, *ipso*-C*H* of Cy, $[HNMe_2(CH_2)_{17}CH_3]^+$), 0.06 (s, 18H, Si*Me*$_3$); ^{13}C NMR

(100 MHz, $CDCl_3$, 25 °C) δ 42.26, 42.17 ([HN*Me*$_2$(*n*-octadecyl)]$^+$), 31.99, 29.77, 29.68, 29.43, 22.77 ([HNMe$_2$-(*C*H$_2$)$_{17}$CH$_3$]$^+$), 28.25, 28.20, 28.15, 28.05, 28.01, 27.87, 27.73, 27.72, 27.67, 27.57, 27.55, 27.44, 27.36, 27.30, 27.24, 27.21, 27.16, 27.09, 27.06, 27.03, 26.96, 26.93, 26.89 (*C*H$_2$ of Cy), 25.22, 25.19, 24.80, 24.16, 23.80, 22.84, 22.61 (*ipso-C*H of Cy), 14.20 ([HNMe$_2$(CH$_2$)$_{17}$*C*H$_3$), 2.23 (Si(*C*H$_3$)$_3$); ^{29}Si NMR (76 MHz, $CDCl_3$, 0.02 M Cr(acac)$_3$, 25 °C) δ 8.06, −64.54, −64.67, −65.08, −65.28, −65.53, −67.98, −68.17. Anal. Calcd for $C_{96}H_{188}O_{24}NSi_{16}Al$ (2216.89): C, 52.01; H, 8.55; N, 0.63%. Found C, 51.99; H, 8.60; N, 0.66%.

2.1.1.4. ***2f*** *([Y]$^+$ = [HNC$_5$H$_5$]$^+$, R = allyl).* Yield 61%. ^{1}H NMR (400 MHz, $CDCl_3$, 25 °C) δ 9.19 (br, 2H), 8.27 (br, 1H), 7.81 (br, 2H, [HNC$_5$*H*$_5$]$^+$), 5.64–5.53 (m, 2H, SiMe$_2$-CH$_2$C*H*=CH$_2$), 4.73 (br m, 4H, SiMe$_2$CH$_2$CH=C*H*$_2$), 1.73–1.19 (br m, 112H, C*H*$_2$ of Cy), 0.93 (d, $^3J_{HH}$ = 9.2 Hz, 4H, SiMe$_2$C*H*$_2$CH=CH$_2$), 0.91–0.79 (br m, 14H, *ipso*-C*H* of Cy), −0.14 (s, 6H, Si*Me*$_2$CH$_2$CH=CH$_2$), −0.32 (s, 6H, Si*Me*$_2$CH$_2$CH=CH$_2$); ^{13}C NMR (100 MHz, $CDCl_3$, 25 °C) δ 143.91, 143.84, 126.34 ([HN*C*$_5$H$_5$]$^+$), 133.95 (SiMe$_2$CH$_2$*C*H=CH$_2$) 113.42 (SiMe$_2$CH$_2$CH=*C*H$_2$) 28.12, 28.03, 27.95, 27.93, 27.87, 27.78, 27.76, 27.69, 27.59, 27.57, 27.48, 27.22, 27.20, 27.16, 27.12, 27.07, 27.04, 27.02, 26.98 (*C*H$_2$ of Cy), 26.05 (SiMe$_2$*C*H$_2$CH=CH$_2$), 24.92, 24.84, 24.21, 24.01, 23.79, 22.83, 22.69 (*ipso-C*H of Cy), −0.39, −0.60 (Si*Me*$_2$CH$_2$CH=CH$_2$); Anal. Calcd for $C_{85}H_{154}O_{24}NSi_{16}Al$ (2050.50): C, 49.79; H, 7.57; N, 0.68%. Found C, 49.18; H, 7.50; N, 0.51%.

2.1.2. Synthesis of [HNC$_5$H$_5$]$^+$[{(c-C$_5$H$_9$)$_8$Si$_8$O$_{13}$}$_2$Al]$^-$ ***(3d)***

A similar method for **2b–h** was adopted by using (*c*-C$_5$H$_9$)$_7$Si$_8$O$_{11}$(OH)$_2$ (2.0 mmol) instead of (*c*-C$_5$H$_9$)$_7$Si$_7$-O$_{10}$(SiMe$_3$)(OH)$_2$. Yield 52%. ^{1}H NMR (400 MHz, $CDCl_3$, 25 °C) δ 8.84 (br m, 2H), 8.25 (br m, 1H), 7.74 (br m, 2H, [HNC$_5$*H*$_5$]$^+$), 1.66–1.34 (br m, 128H, C*H*$_2$ of Cy), 0.94–0.60 (br m, 16H, C*H* of Cy); ^{13}C NMR (100 MHz, $CDCl_3$, 25 °C) δ 125.74 ([HN*C*$_5$H$_5$]$^+$), 28.01, 27.66, 27.63, 27.37, 27.23, 27.17, 27.12, 27.09 (*C*H$_2$ of Cy), 24.92, 23.19, 22.50 (*ipso-C*H of Cy); ^{29}Si NMR (76 MHz, $CDCl_3$, 0.02 M Cr(acac)$_3$, 25 °C) δ −65.68, −66.96, −68.99. Anal. Calcd for $C_{85}H_{150}O_{26}NSi_{16}Al$ (2078.47): C, 49.12; H, 7.27; N, 0.73%. Found C, 48.37; H, 6.96; N, 0.62%.

2.1.3. Synthesis of [HNC$_5$H$_5$]$^+$[{(i-C$_4$H$_9$)$_8$Si$_8$O$_{13}$}$_2$Al]$^-$ ***(4d)***

A similar method for **3d** was adopted by using (*i*-C$_4$H$_9$)$_7$Si$_8$O$_{11}$(OH)$_2$ (2.0 mmol) instead of (*c*-C$_5$H$_9$)$_7$Si$_8$-O$_{11}$(OH)$_2$. Yield 45%. ^{1}H NMR (400 MHz, $CDCl_3$, 25 °C) δ 8.82 (br m, 2H), 8.24 (br m, 1H), 7.70 (br m, 2H, [HNC$_5$*H*$_5$]$^+$), 1.84–1.70 (br m, 16H, CH$_2$C*H*(CH$_3$)$_2$), 0.93–0.82 (br m, 96H, CH$_2$CH(C*H*$_3$)$_2$), 0.54–0.33 (br m, 32H, C*H*$_2$CH(CH$_3$)$_2$); ^{13}C NMR (100 MHz, $CDCl_3$, 25 °C) δ 125.71 ([*C*$_5$H$_5$NH]$^+$), 26.18, 25.98, 25.78 (CH$_2$*C*H-(CH$_3$)$_3$), 24.96, 23.65, 22.74 (*C*H$_2$CH(CH$_3$)$_2$), 24.39, 24.11, 23.99 (CH$_2$CH(*C*H$_3$)$_2$); ^{29}Si NMR (76 MHz, $CDCl_3$, 0.02 M Cr(acac)$_3$, 25 °C) δ −66.94, −67.28, −69.78. MS (FAB) *m*/*z* 1749 (95) [M–C$_4$H$_9$ + H]$^+$, 1961 (100) [M–2C$_4$H$_9$]$^+$. Anal. Calcd for $C_{69}H_{150}O_{26}NSi_{16}Al$ (1886.29): C, 43.94; H, 8.02; N, 0.74%. Found C, 43.62; H, 7.61; N, 0.69%.

2.1.4. Synthesis of [(t-C$_4$H$_9$O)$_3$SiO]$_3$Al · pyridine ***(5)***

To a hexane solution (70 cm^3) of (*t*-C$_4$H$_9$O)$_3$SiOH (2.0 mmol) was added dropwise a hexane solution (1.0 cm^3) of triethylaluminum (1 M, 1.0 mmol) at 0 °C. Pyridine (1.2 mmol) was added at 0 °C, followed by stirring at room temperature for 24 h. After removal of the solvent, recrystallization by slow diffusion of acetone into the toluene solution afforded colorless crystals of **5**. Note that [(*t*-C$_4$H$_9$O)$_3$SiO]$_3$Al · THF has been synthesized by the reaction of (*t*-C$_4$H$_9$O)$_3$SiOH and aluminum triisopropoxide in THF [40]. Yield 67%. ^{1}H NMR: δ 7.50, 7.97, 9.25 (2H, 1H, 2H, NC$_5$*H*$_5$), 1.23 (81H, –OC(C*H*$_3$)$_3$). ^{13}C{^{1}H}NMR: δ 124.15, 140.40, 149.23 (N*C*$_5$H$_5$), 71.28 (–O*C*(CH$_3$)$_3$), 31.53 (–OC(*C*H$_3$)$_3$). ^{29}Si{^{1}H}NMR: δ −97.11 (–*Si*OC-(CH$_3$)$_3$). Anal. Calcd for $C_{41}H_{86}NO_{12}Si_3Al$ (896.36): C, 54.94; H, 9.67; N, 1.56%. Found C, 54.29; H, 9.55; N, 1.52%.

2.2. Preparations of oxides from silsesquioxanes

Calcination of group 13 element-containing silsesquioxanes (typically 0.50 g) was performed in a stream of dried, CO_2-free air (W/F = 5.0 g h mol^{-1}) by using a fixed-bed flow-type quartz reactor (i.d. 8.0 mm) under atmospheric pressure. Temperature was usually raised by 10 K min^{-1} to the prescribed level and held for 4 h. Calcined samples were carefully recovered with minimal contact with air and moisture and stored under an argon atmosphere. The reference catalysts were calcined at 823 K in the same manner just before the use.

2.3. Analysis

The NMR data were obtained on JEOL JNM-AL-300 spectrometer (FT, 300 MHz (^{1}H), 75 MHz (^{13}C)) or on JEOL JNM-EX-400 spectrometer (FT, 400 MHz (^{1}H), 100 MHz (^{13}C), 76 MHz (^{29}Si)), respectively. Chemical shifts are reported relative to tetramethylsilane. Correlation and assignment of ^{1}H and ^{13}C NMR resonances were aided by DEPT and 2D COSY experiments when necessary. Fast atomic bombarding (FAB) mass spectra of silsesquioxanes were recorded using a JEOL SX-102A mass spectrometer. 2-Nitrophenyl octyl ether was used as the matrix. Elemental analyses were performed at the Microanalytical Center of Kyoto University. TG and DTA analyses were done by using a Shimadzu DTA-50 analyzer in a stream of synthesized air or dry nitrogen (40 cm^3 min^{-1} for typically 15 mg of silsesquioxanes). FTIR spectra of silsesquioxanes and heat-treated samples were recorded on a Nicolet Impact 410 spectrometer.

The resulting oxides were analyzed by nitrogen gas adsorption, XRD, FTIR, XPS, SEM, EPMA, ammonia TPD, and so on. Nitrogen adsorption/desorption isotherms were obtained with a Quantachrome Autosorb 1-MP, a computer-controlled automatic gas sorption system. Samples were degassed at 473 K for 2 h just before the measurements. XRD (X-ray diffraction) study was performed using a Shimadzu XD-D1 with $K_{\alpha_{1,2}}$ emission of copper in the range $5° < 2\theta < 70°$. XPS (X-ray photoelectron spectra) of the catalysts were acquired using an ULVAC-PHI 5500MT system equipped with a hemispherical energy analyzer. Samples were mounted on indium foil and then transferred to an XPS analyzer chamber. The residual gas pressure in the chamber during data acquisition was less than 1×10^{-8} Torr (1 Torr = 133.3 N m^{-2}). The spectra were measured at room temperature using Mg $K_{\alpha_{1,2}}$ radiation (15 kV, 400 W). The electron take-off angle was set at 45°. Binding energies were referenced to C 1s level of residual graphitic carbon. The apparent shape and size of the oxide particles were observed by using a Hitachi S-2500 CX scanning electron microscope (SEM). EPMA analyses were also performed by using a spot energy differential X-ray analyzer, HORIBA EMAX 5770.

Temperature-programmed desorption (TPD) of ammonia was measured using a TPD-1-AT apparatus (BEL Japan). After the sample was in a flow of He (50 cm^3 min^{-1}) at 723 K for 30 min, it was exposed to NH_3 (1.3 N m^{-2}) 373 K for 30 min at 373 K. The sample was subsequently evacuated at 373 for 6 h to remove physisorbed ammonia. The temperature of the sample was raised at a rate of 10 K min^{-1} to 1073 K. Mass number 16 was monitored to evaluate the amount of desorbed ammonia. Calibration of the sensitivity toward ammonia was done just after each experiment.

2.4. Cracking of hydrocarbons

The catalytic activities of the oxides for the cracking of hydrocarbons, cumene and *n*-propylbenzene, were performed using a flow reactor at 523–773 K, at ordinary pressure. Thirty milligrams of catalyst was loaded in a quartz reactor (i.d. 3.0 mm). Cumene or *n*-propylbenzene (2.0 µl, 14 µmol) was injected into the He carrier gas stream (40 cm^3 min^{-1}) for one pulse, and this procedure was repeated 7 times at 30-min intervals. Products and the unreacted hydrocarbon were analyzed by means of on-line TCD gas chromatograph (Shimadzu GC-8A) using a column (i.d. 3.0 mm, 3.0 m) packed with silicone SE-30.

3. Results and discussion

3.1. Synthesis of new aluminum-bridged silsesquioxanes

New derivatives of aluminum-bridged silsesquioxanes with various counter ammonium cations, including very bulky ones, were prepared based on the method reported for **2a** and **2d** [15,16] (see Eq. (1)).

The reaction of silsesquioxane disilanol, $(c\text{-}C_5H_9)_7Si_7O_{10}(RSiMe_2)(OH)_2$ (R = Me, vinyl, allyl) with trimethylaluminum in hexane solution followed by the addition of amine at 0 °C cleanly proceeded, and after recrystallization, the desired aluminum-bridged silsesquioxanes are isolated in moderate yields.

The structures of these molecules are deduced on the basis of ^{1}H, ^{13}C, and ^{29}Si NMR, and FAB-MASS spectra. These data are consistent with their structures shown in Eq. (1). The ^{13}C NMR spectrum of **2c** bearing a dimethyloctylammonium cation suggests the presence of hydrogen bondings between the ammonium cation and the silsesquioxane anion even in solution. There are two signals (42.26 and 42.16 ppm) of methyl carbons in the ammonium cation, indicating the magnetic inequivalence of these two methyl groups. The strong interaction of the cation with the locally C_2 symmetric silsesquioxane anion can be the rationalize for this observation. On the other hand, similar to the case with other group 13 element-bridged silsesquioxanes [15,16,28,29], the ^{29}Si NMR spectra consist of eight peaks of almost the same intensity for 16 silicon atoms, which indicates apparent local C_2 symmetry of their siloxane framework. This indicates that the presence of the anion nearby the bridging oxygen only slightly affects the NMR resonances of the anionic siloxane framework.

The preliminary X-ray study of **2d** demonstrated that the distance between a nitrogen atom of the pyridinium

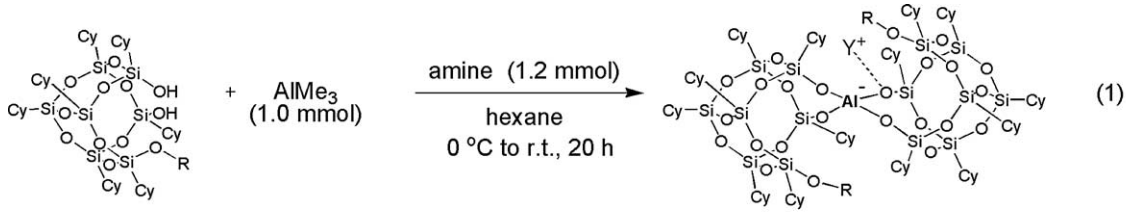

(Cy = *c*-C_5H_9,
R = $SiMe_3$, $SiMe_2$(allyl))
(2.0 mmol)

2a (R = $SiMe_3$, Y^+ = $[HNEt_3]^+$)
2b (R = $SiMe_3$, Y^+ = $[H_2NEt_2]^+$)
2c (R = $SiMe_3$, Y^+ = $[HNMe_2(n\text{-octyl})]^+$)
2d (R = $SiMe_3$, Y^+ = $[HNC_5H_5]^+$)
2e (R = $SiMe_3$, Y^+ = $[HNMe_2(n\text{-octadecyl})]^+$)
2f (R = $SiMe_2$(allyl), Y^+ = $[HNC_5H_5]^+$)
2g (R = $SiMe_3$, Y^+ = H^+)

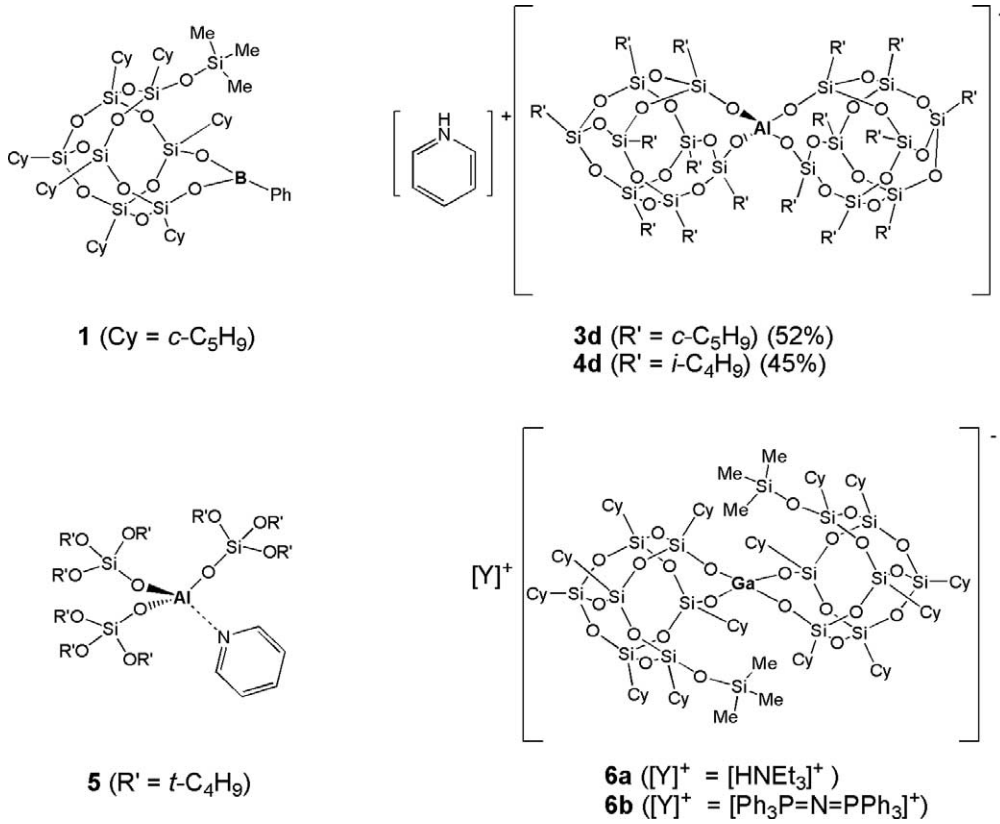

Scheme 1.

cation and an oxygen atom of one Al–O–Si bonding is very short, 2.75(4) Å, indicating the presence of strong hydrogen bonding between ammonium cations and bridging oxygen atoms [16]. The observations in the NMR and X-ray diffraction measurements clearly suggest the presence of strong interaction of the ammonium cation and the silsesquioxane anion of **2a**–**f**, both in the solid state and in solution. Unfortunately, lack of diffractions at high 2θ angles hampered the complete solution of the structure of **2d**. Colorless single crystals of **2d** were obtained by slow diffusion of acetonitrile into a toluene solution, which has the monoclinic space group Cc. The cell constants were a, 22,365(2) Å; b, 14,977(1) Å; c, 32,083(3) Å; β, 91,783(2)°; $V = 10741(1)$ Å^3. At present only isotropical refinement has been achieved because of its poor diffractions in the high angle region of $2\theta > 30°$. Note that the X-ray crystallographic study has been performed on $[HNEt_3]^+\{Al[(Me_3SiO)(c\text{-}C_6H_{11})_7Si_7O_{11}]_2\}^-$ [15] and **2a** [16]. In the former case, a triethylammonium cation was reported to be located far from the aluminum center, while in the structure of **2a** the ammonium cation was found to be just alongside the bridging oxygen atoms as shown in our X-ray study. This indicates that the position of ammonium cation is very sensitive to the peripheral organic substituents of the silsesquioxane.

The reactions of silsesquioxane disilanols, $(c\text{-}C_5H_9)_8Si_8O_{11}(OH)_2$ and $(i\text{-}C_4H_9)_8Si_8O_{11}(OH)_2$, with trimethylaluminum in the presence of pyridine cleanly produce the corresponding aluminum-bridged molecules, **3d** and **4d**, respectively (Scheme 1) [17]. Their structures are deduced on the basis of ^{1}H, ^{13}C, and ^{29}Si NMR, and FAB-MASS spectra. The ^{1}H NMR spectra of these molecules show the presence of two half-cage silsesquioxane cores and one ammonium cation. The ^{13}C NMR spectrum shows three sets of resonances in a 1:2:1 ratio for the carbon atoms in peripheral groups, which is consistent with the structure shown in Scheme 1. For **3d** and **4d**, however, the presence of hydrogen bondings between the cations and anions has not been confirmed by the NMR measurements. The FAB-MASS spectrum of **4d** shows distinct $[M–(alkyl) + H]^+$ peaks, and their isotropic distribution patterns are consistent with their molecular compositions.

For comparison, a pyridine-stabilized Lewis acidic siloxyaluminum compound, $[(t\text{-}C_4H_9O)_3SiO]_3Al \cdot$ pyridine (**5**), is synthesized. The group 13 element-containing silsesquioxanes, **1**, **6a**, and **6b**, are also prepared [29]. The reaction of triethylaluminum and more than 4 eq of $(t\text{-}C_4H_9O)_3SiOH$ in the presence of excess pyridine in hexane solution at 0 °C yields **5** in place of the expected pyridine-stabilized Brønsted acidic products. All spectra are consistent with those reported for $[(t\text{-}C_4H_9O)_3SiO]_3Al \cdot$ THF [40]. As one reason for the absence of Brønsted acidic-type products, the steric hindrance of bulky $(t\text{-}C_4H_9O)_3SiO–$ groups which hampers the reaction of the aluminum center with the fourth $(t\text{-}C_4H_9O)_3SiOH$ can be considered.

Table 1
Effect of calcination temperature on the pore texture of the oxides from silsesquioxanes

Oxides[a]	BET surface area ($m^2\,g^{-1}$)	Total pore volume ($cm^3\,g^{-1}$)	Carbon deposition
2a-523	< 2	< 0.01	++
2a-573	500	0.22	++
2a-623	500	0.22	++
2a-673	510	0.23	++
2a-723	520	0.23	++
2a-773	490	0.22	+
2a-823	460	0.20	–
2a-923	360	0.16	–

[a] All samples were evacuated at 473 K for 2 h just before the measurement. Numbers represent the calcination temperature (K).

3.2. Catalytic activities of the oxides from aluminum-bridged silsesquioxanes for the cracking of hydrocarbons

Aluminum species in the silsesquioxanes described above are atomically dispersed, and these elements are expected to be bonded or at least to stay close to the siloxane cages even under oxidative atmosphere at high temperatures. If four Al–O–Si bondings around each aluminum atoms are kept intact, Brønsted acidic sites will be produced by the calcinations. Therefore, the properties and catalytic activities of the oxides prepared from aluminum-bridged silsesquioxanes for the cracking of hydrocarbons have been examined. For comparison, activities of the oxides from **1**, **6a**, and **6b** have also been tested.

As shown in the previous report, controlled calcination of **1**, **2a**, **6a**, and **6b** in air flow produced porous M–Si–O materials (M = B, Al, Ga) with large surface areas (300–500 $m^2\,g^{-1}$) and uniformly controlled micropores (ca. 5–6 Å) [29]. Porous oxides of similar pore textures have been also produced by the calcination of newly synthesized silsesquioxanes, **2b**–**f**, **3d**, and **4d**. Table 1 summarizes specific surface areas and total pore volumes of the oxides prepared by the calcination of **2a** at various temperatures. The oxide derived from **2a** at 823 K is further designated as **2a**-823. The calcination at temperature below 523 K produced black solids with small surface areas of less than 2 $m^2\,g^{-1}$, while at higher temperatures areas as high as 500 $m^2\,g^{-1}$ are achieved. On the surface of the oxides prepared at lower than 723 K, however, severe deposition of carbonaceous materials was observed, which significantly reduces the catalytic activities of the oxides. On the other hand, treatment at temperatures higher than 823 K significantly reduces their surface areas. Eventually, calcination at around 823 K produces white oxides with large surface areas of 460 $m^2\,g^{-1}$.

Table 2 shows the effect of precursors on the surface areas. While **2c**-823, **2d**-823, and **2f**-823 show surface areas as high as that of **2a**-823, the oxides from **2b** and **2e** possess lower surface areas. The silsesquioxanes bearing cages of different structures, **3d** and **4d**, also show high surface areas (440–470 $m^2\,g^{-1}$). The difference in peripheral organic substituents only slightly affects the surface areas. The oxide from Brønsted acidic **2g** shows the surface area of 340 $m^2\,g^{-1}$, slightly lower than the previously reported value [32]. Although direct calcination of **5** results in the formation of nonporous materials (**5**-823), calcination of **5** after the gelation at 373 K under vacuum for 14.5 h produces the mesoporous oxide (**5**-823G, mean pore diameter = 200 nm) with high surface areas. Similar results have been previously reported by Tilley et al. [40].

Table 2
Effect of silsesquioxanes on the pore texture of the oxides

Oxides[a]	BET surface area ($m^2\,g^{-1}$)	Total pore volume ($cm^3\,g^{-1}$)
2a-823	460	0.20
2b-823	340	0.14
2c-823	450	0.19
2d-823	520	0.22
2e-823	350	0.15
2f-823	500	0.21
2g-823[b]	340	0.14
3d-823	470	0.19
4d-823	440	0.19
5-823	20	0.01
5-823G[c]	750	0.33

[a] All samples were evacuated at 473 K for 2 h just before the measurement. Numbers represent the calcination temperature (K).
[b] **2g**-823 has been prepared by Maxim et al. [32].
[c] Calcined after gelation at 373 K for 14.5 h.

As shown in Fig. 1, the nitrogen adsorption/desorption isotherms of the oxides from **2b**–**f**, **3d**, and **4d** shows typical type I isotherms [41], characteristic of microporous materials prepared by the calcination of silsesquioxanes [25–34]. There are no significant effects of countercations, cage shapes, and peripheral organic substituents on the "shape" of isotherms. The adsorbed volume of **5**-823 is very low, while **5**-823G shows the typical isotherm of mesoporous materials [41].

We assumed that the sterically demanding countercations might affect the pore textures, since countercations are considered to stay nearby the silsesquioxane anions. Pore-size distributions estimated from the nitrogen adsorption isotherms by the Saito-Foley method [42] (Fig. 2) are, however, not affected by the countercations. The oxide from **2e**, which includes a bulky dimethyloctadecylammonium cation, shows a peak at around 5.5 Å.

Note that the XRD spectra of **2a**–**f**-823 consist of only one broad band at around $2\theta = 23°$. This indicates that all oxides examined are amorphous. SEM analyses of the oxides from aluminum-bridged silsesquioxanes show the formation of large cubic particles (ca. 30 × 30 × 30 μm), while **5**-823 and **5**-823G consist of smaller particles (ca. 0.1 μm in diameter). The formation of discrete particles of aluminum oxide was not recognized by SEM-EDX analysis in all cases examined.

In order to examine the reason why the cations of silsesquioxanes do not influence the pore sizes of the oxides, thermogravimetric analysis was performed (Fig. 3). An

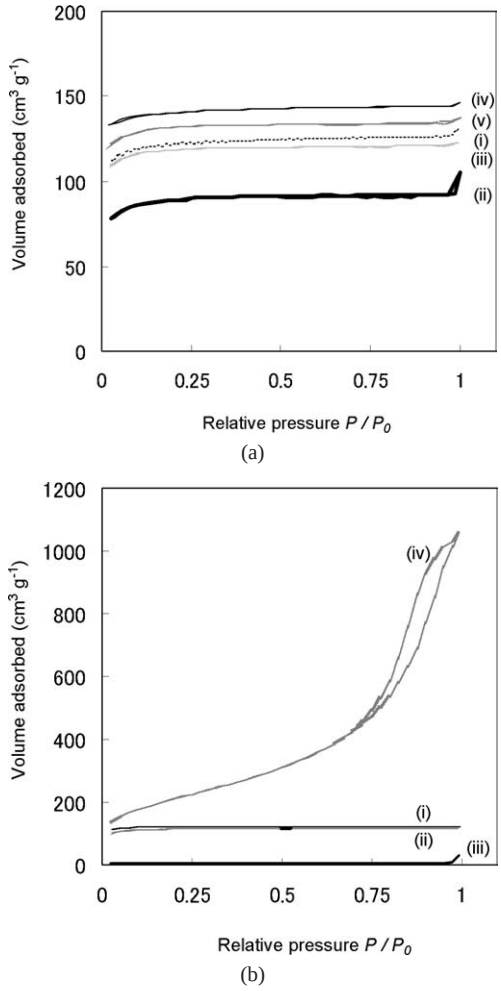

Fig. 1. (a) Nitrogen isotherms of the oxides prepared from silsesquioxanes. (i) **2a**-823, (ii) **2b**-823, (iii) **2c**-823, (iv) **2d**-823, (v) **2f**-823. (b) Nitrogen isotherms of the oxides prepared from silsesquioxanes. (i) **3d**-823, (ii) **4d**-823, (iii) **5**-823, (iv) **5**-823G.

aluminum-bridged silsesquioxanes **2d** shows weight losses in three steps. The first endothermic decrease in its weight by ca. 5%, due to the decomposition of the pyridinium cation, was observed at around 500 K. The second-step marked weight decrease which occurred at 523–723 K is exothermic. This is probably due to the thermal decomposition of peripheral cyclopentyl rings together with the formation of carbonaceous deposits. The final significantly exothermic weight decrease at above 723 K is considered to be responsible for the combustion of the remaining carbonaceous materials. This observation is also true for other silsesquioxanes, **2a** and **2e**. The present results suggest that ammonium cations are eliminated from the solid *before* the formation of micropores.

Irrespective of the kinds of precursor molecules, the pore sizes of the oxides in the present study are within the range found in the porous materials prepared by the thermal treatment of discrete silsesquioxane molecules, including metallic species or not [26–34], and silsesquioxane polymers [43,44]. And the pore texture of the resulting oxides

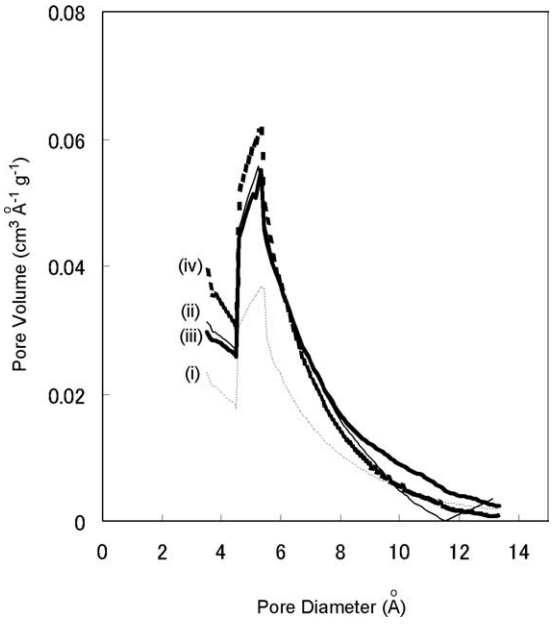

Fig. 2. Pore-size distribution of the oxides estimated by the Saito–Foley method based on the nitrogen isotherms. (i) **2b**-823, (ii) **2c**-823, (iii) **2d**-823, (iv) **2f**-823.

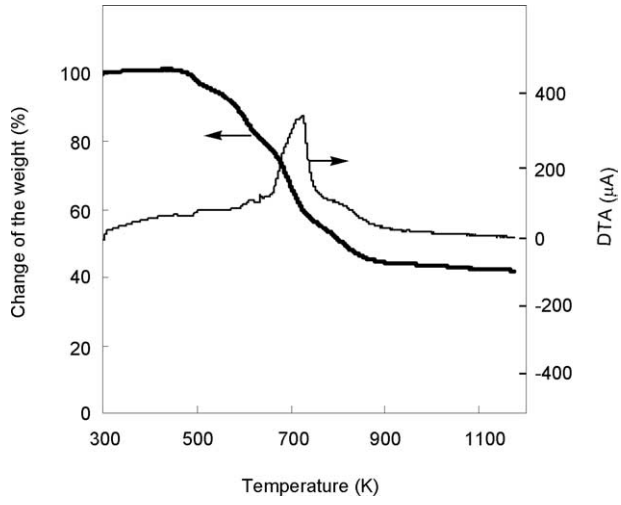

Fig. 3. Thermogravimetric analysis of an aluminum-bridged silsesquioxane **2d**.

is not much influenced by the kind of precursor silsesquioxanes, indicating the intrinsic difficulty of tailoring the pore sizes. However, tailoring the pore sizes by the introduction of more thermally stable directing ligands or highly reactive functional groups for polymerization at low temperatures into the silsesquioxane molecules is still considered to be possible. Attempts are now ongoing.

The FTIR study of the heat-treated **2d** also supports the above discussion (Fig. 4). As the treatment temperature increased above 523 K, the relative intensity of the bands assigned to $\upsilon_{C–H}$ and $\sigma_{C–H}$ vibrations due to peripheral cyclopentyl groups decreased, and almost completely disappeared at above 623 K. In their place, several new bands

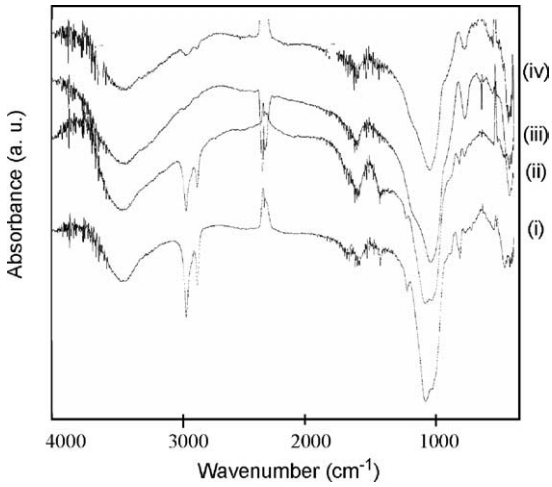

Fig. 4. FTIR spectrum of the solid materials prepared from an aluminum-bridged silsesquioxane. (i) **2d**-523, (ii) **2d**-573, (iii) **2d**-623, (iv) **2d**-673.

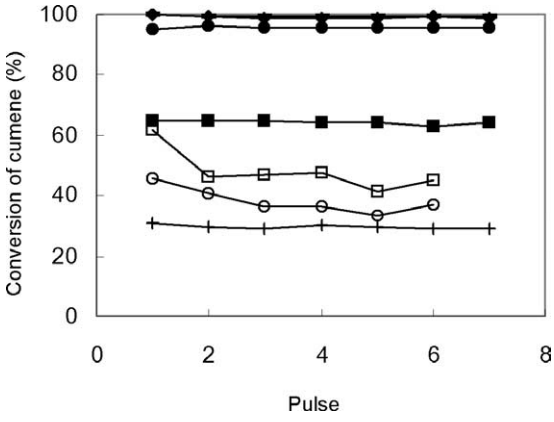

Fig. 5. Activity of oxide catalysts prepared from group 13 element-containing silsesquioxanes for the cracking of cumene at 673 K. **2a**-823 (◆), **2a**-923 (●), **6a**-823 (□), **6a**-923 (○), **6b**-823 (+), JRC-Z5-H90 (–), CCIC-LA (■).

corresponding to Si–O bondings emerged at this temperature. This indicates that the decomposition of the cyclopentyl rings occurs at around 623–673 K together with the formation of new Si–O–Si bondings.

The cracking of model hydrocarbons, especially cumene, is often examined in order to investigate the ability of the solid acidic catalysts [1,45]. As shown in the following figures, the catalytic activities of the oxides prepared from group 13 element-containing silsesquioxanes toward the cumene cracking reactions were performed using a pulse reactor. The observed products were benzene and propene. Other products except for a trace amount of methane were not observed. Figs. 5 to 9 compare the catalytic activities of various aluminum and gallium-containing oxides at 523–673 K. The activities of a zeolite and a commercial aluminosilicate CCIC-LA (BET surface area = 570 $m^2\,g^{-1}$, pore volume = 0.71 $cm^3\,g^{-1}$, alumina 13.5%) are also shown for comparison. The zeolite JRC-Z5-90H is selected because it possesses a similar amount of acidic sites to the oxides

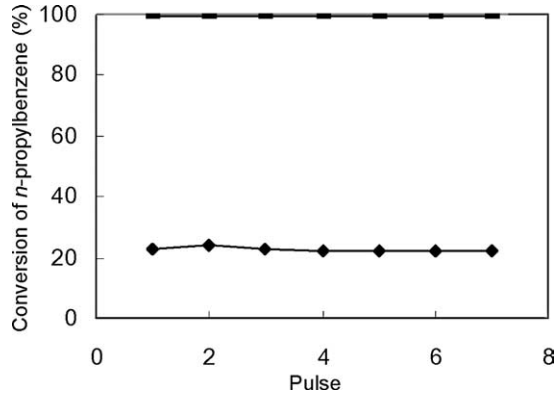

Fig. 6. Activity of aluminum-bridged silsesquioxane-based catalysts for the cracking of *n*-propylbenzene at 673 K. **2a**-823 (◆), JRC-Z5-H90 (–).

from aluminosilsesquioxanes (0.362 mmol g^{-1} for JRC-Z5-90H, and 0.350 mmol g^{-1} for **2d**-823, see below), so that the activities of acidic sites on these catalysts can be directly compared.

At 673 K (Fig. 5), aluminum-containing oxide catalysts, **2a**-823 and **2a**-923, as well as JRC-Z5-90H show excellent activities. Almost 100% conversion of cumene has been achieved. On the other hand, the use of commercial amorphous aluminosilicate, CCIC-LA results in ca. 60% of initial conversion of cumene. The gallium-containing porous oxides, **6a**-823, **6a**-923, and **6b**-823, were not very effective. The conversions of cumene were less than 60%. The decline of the catalytic activity of **6a**-823 with increasing number of pulses was observed. The surface of this catalyst turned black during the reaction because of the coke formation. It has been found that **6a**-823 contains not only weak acidic sites but also very strong acidic sites [29], probably the Lewis acidic sites due to the gallium species isolated from silica matrices [46]. These strong acidic sites are considered to be responsible for the severe deposition of coke [46]. Note that boron-containing oxide did not show any significant activities for this reaction even at higher temperatures.

The activity of aluminum-containing oxides toward the cracking of *n*-propylbenzene at 673 K was also examined (Fig. 6). While with the HZSM-5 zeolite complete conversion of *n*-propylbenzene to benzene and propene was achieved, the conversion by the use of **2a**-823 was low, ca. 20%. This shows that the strength of the acidic sites is sufficient for the cracking of cumene but not for less basic *n*-propylbenzene (see below).

At 573 K (Fig. 7), the catalyst **2a**-823 shows the initial cumene conversion of ca.70%, whereas almost complete conversion of cumene has been achieved by the use of the JRC-Z5-90H catalysts, indicating that the innate activity of **2a**-823 is somewhat lower than that of the zeolites. The oxide **2a**-923 shows lower activity than that of **2a**-823. The significantly lower BET surface area of **2a**-923 would be one reason. At this reaction temperature, the oxides prepared from gallium-containing silsesquioxanes do not show significant activities.

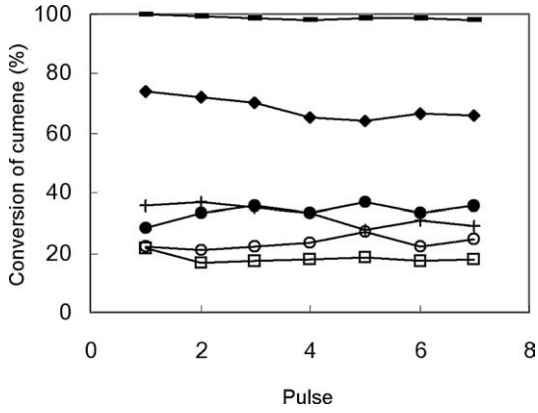

Fig. 7. Activity of oxide catalysts prepared from group 13 element-containing silsesquioxanes for the cracking of cumene at 573 K. **2a**-823 (◆), **2a**-923 (●), **6a**-823 (□), **6a**-923 (○), **6b**-823 (+), JRC-Z5-H90 (–).

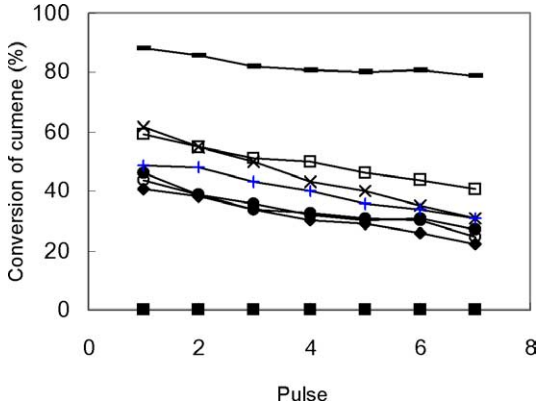

Fig. 8. Activity of aluminum-bridged silsesquioxane-based catalysts for the cracking of cumene at 523 K. **2a**-823 (◆), **2b**-823 (○), **2c**-823 (×), **2d**-823 (□), **2e**-823 (●), **2g**-823 (+), JRC-Z5-H90 (–), CCIC-LA (■).

The activities of the oxides from various aluminosilsesquioxanes were compared at 523 K (Fig. 8). At this temperature, commercial amorphous aluminosilicate catalysts do not show cracking activities. The oxides from aluminum-bridged silsesquioxanes show moderate activities, although they are slightly less active than the HZSM-5 zeolite. There are slight decreases in their activities with increasing numbers of pulses, probably due to the slight coke formation on the catalyst as is observed after the catalytic runs. Fig. 8 also shows the effect of the countercations of the precursors on the activities of the resulting oxides. Among the samples examined, silsesquioxanes including *N*,*N*-dimethyloctylammonium or pyridinium cation (**2c** and **2d**, respectively) are found to be effective precursors for the cracking catalysts. The evaluation of the activity of **2g**-823 is not straightforward. The conversion significantly changes in each repeated run, and sometimes the oxide does not show any activity. At the present time we assume that the relatively low stability of **2g** against heat, air, and moisture would make the preparation of oxides extremely sensitive to the calcination conditions and storage conditions. Note that

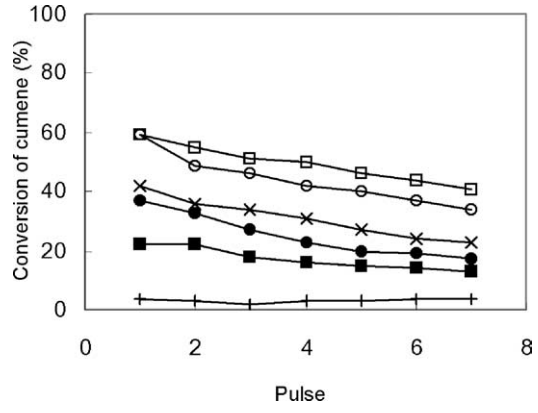

Fig. 9. Effect of the structure of silsesquioxanes on the catalytic activity of oxides toward the cracking of cumeneat 523 K. **2d**-823 (□), **2f**-823 (○), **3d**-823 (×), **4d**-823 (●), **5**-823 (+), **5**-823G (■).

Table 3
XPS analysis of the oxides prepared from aluminum-bridged silsesquioxanes

Oxides	Surface composition					Binding energy (eV)
	Si (%)	Al (%)	O (%)	C (%)	Si/AI	Al 2p
2a-823	28.29	1.87	63.03	6.81	15.1	75.0
2b-823	26.59	1.46	61.54	10.42	18.2	74.8
2c-823	29.15	1.76	67.05	2.03	16.7	74.2
2d-723	27.64	1.74	64.02	6.34	15.9	74.4
2d-823	28.26	1.83	66.94	2.97	15.4	74.4
2e-823	27.28	1.80	66.09	4.44	15.2	74.4
3d-823	28.41	1.82	65.40	4.08	15.6	74.4
5-823	22.17	6.64	63.27	7.06	3.34	74.0
Al_2O_3[a]						74.0

[a] Binding energy of alumina reported in the literature [47].

with regard to oxides other than those from **2g** the activities are highly reproducible.

Fig. 9 shows the comparison of the catalytic activities of the oxides prepared from aluminum-containing precursors of different structures. The activities of nonporous or mesoporous oxides prepared from **5** were also examined. The presence of allyldimethylsilyl groups in the precursor molecule (**2f**) has a slightly negative effect. The oxides prepared from an aluminum-bridged molecule of different structure, **3d**-823, also shows lower activity. The activity of **4d**-823 bearing peripheral isobutyl groups in place of cyclopentyl groups also results in lower yields of the product. These results indicate that **2c** and **2d** are mostly appropriate precursors for the preparation of active cracking catalysts. On the other hand, mesoporous oxide **5**-823G shows significantly lower activity than **2d**-823 despite its higher BET surface area. This again indicates that molecules bearing four Si–O–Al bondings are more suitable precursors for the cracking catalysts than amine-stabilized Lewis acidic-type molecules such as **5**. The present study clearly shows the exceptionally high activity of the oxides from aluminum-bridged silsesquioxanes despite their amorphous nature.

The state of aluminum species on the catalytically active oxides prepared from aluminosilsesquioxanes was ex-

amined. Table 3 summarizes the results of the XPS study of aluminum-containing silsesquioxanes. The surface atomic ratios are calculated based on the sensitivity factors reported for the spectrometer used in this study [47]. The ratio of Si/Al on the surfaces of **2c**-823, **2d**-823, and **2h**-823, as well as **2a**-823, is about 15 to 16, almost similar to their bulk Si/Al ratios (about 15). On the other hand, a higher ratio of 18.2 was observed for **2b**-823. According to the previous discussion in the study of supported molybdenum catalysts [48,49], a higher surface Si/M ratio could be an indication of lower dispersion of the metallic species.

The Al 2p peaks of the oxides prepared from aluminum-bridged silsesquioxanes were significantly shifted toward the higher binding energy side (74.2–75.0 eV) from the reported value for γ-Al_2O_3 (74.0 eV) [47], whereas **5**-823 show their Al 2p peak at 74.0 eV. The previous extensive report on the thin layer of silica deposited on alumina shows that a similar shift is responsible for the Al–O–Si bonds in high dispersion [50]. These phenomena have been also reported for titanosilicates or silica–titania catalysts and assigned to the elements surrounded by electron-withdrawing siloxane frameworks [51]. The present results suggest that the aluminum species in the oxides prepared from aluminum-bridged silsesquioxanes are atomically dispersed, while those in **2b**-823 are slightly less dispersed. Note that the amounts of carbonaceous species on the surfaces also depend not only on the calcination temperature but also the kind of countercations, while exact reasons are still unclear. Table 3 clearly shows that the calcination at lower temperatures increases the surface ratio of carbon atoms. The surface ratios of carbon atoms in the oxides **2a**-823 and **2b**-823 as well as the oxide calcined at lower temperatures, **2d**-723, are higher than those of other oxides. Their relatively low catalytic activities (see above) are consistent with the idea that remaining carbonaceous materials which cover the surface active sites would be one of the reasons for the decreases in the catalytic activity.

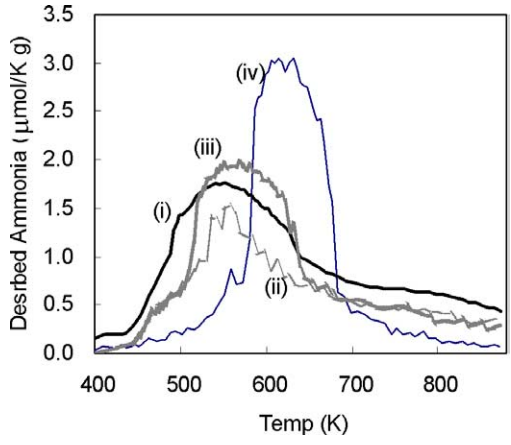

Fig. 10. Ammonia TPD spectra of (i) **2d**-823, (ii) **2d**-723, (iii) **3d**-823, and (iv) JRC-Z5-90H.

The strength and amount of acidic sites were examined by the ammonia temperature-programmed desorption (TPD) study. Fig. 10 shows the TPD spectra of **2d**-823, **2d**-723, **3d**-823, and JRC-Z5-90H. The spectrum of **2d**-823 exhibited a broad band at around 573 K together with a shoulder at higher temperatures, indicating the presence of acidic sites of moderate strength. While the shape of the spectrum is similar to that of **2a**-823 reported in the previous paper [29], much larger amounts of acidic sites are present on the surface of **2d**-823 (0.350 mmol g^{-1}) than **2a**-823 (0.289 mmol g^{-1}). The oxide **3d**-823 also shows a band at around 573 K. The amount of desorbed ammonia from this oxide was 0.271 mmol g^{-1}. These values correspond to about one-third of the amount of aluminum atoms included in these oxides. On the other hand, the oxide prepared at lower temperature, **2d**-723, desorbed a smaller amount of ammonia 0.216 mmol g^{-1}, indicating that al lower calcination temperature greatly decreases the amount of acidic sites. Physical coverage of the acidic sites by the residual carbonaceous materials is one possible reason. Note that the measurements of conventional silica-rich amorphous aluminosilicates by the use of the identical apparatus under the similar conditions show bands at around 473 K [52]. On the other hand, the measurement of JRC-Z5-90H under the identical conditions showed one band at around 623 K (0.362 mmol g^{-1}). The absence of *l* peaks [46] in the spectra, usually observed at around 450 K, indicates the complete elimination of ammonia weakly held on nonacidic sites. In accordance with the desorption temperature of ammonia, the strength of acidic sites on the surface of these oxides is estimated to increase in the following order, conventional amorphous aluminosilicate < oxides from aluminum-bridged silsesquioxanes < JRC-Z5-90H. On the basis of these results, one can estimate that the oxides from aluminosilsesquioxanes possess acidic sites with enough strength for the cracking of cumene even at low reaction temperatures, but they are not acidic enough for the reaction of less-basic *n*-propylbenzene at 673 K (see above).

The ammonium cations of the precursor molecules show a modest influence on the acidic characters and catalytic activities. Although it is hard to find the exact correlation between the catalytic activity and the properties of ammonium cations, i.e., basic characters of their conjugated bases, we estimate that small pyridinium cations can effectively stabilize the Brønsted acidic aluminum-containing silsesquioxanes. The stability of silsesquioxanes would significantly affect the dispersion of aluminum species in the oxides, since the elimination of aluminum species from silsesquioxanes during the calcinations might cause significant segregation of aluminum species.

4. Conclusion

In the present work, we have demonstrated that the controlled calcination of group 13 element-containing silsesqui-

oxanes, including newly prepared $[Y]^+[\{(c\text{-}C_5H_9)_7Si_7O_{12}\text{-}(SiMe_3)\}_2Al]^-$ ($[Y]^+ = [H_2NMe_2]^+$ (**2b**), $[HNMe_2\text{-}(C_8H_{17})]^+$ (**2c**), $[HNMe_2(C_{18}H_{37})]^+$) (**2e**), $[HNC_5H_5]^+\text{-}[\{(c\text{-}C_5H_9)_8Si_8O_{13}\}_2Al]^-$ (**3d**), and $[HNC_5H_5]^+\text{-}[\{(i\text{-}C_4H_9)_8Si_8O_{13}\}_2Al]^-$ (**4d**), at around 823 K produces acidic porous oxides with high BET surface areas and uniformly controlled micropores of 5–6 Å diameter. Remarkably, these oxides prepared from aluminum-bridged silsesquioxanes show excellent catalytic activities toward cumene cracking even at the low temperature, 523 K, whereas commercial silica–alumina catalysts do not show significant activities under the present conditions. Their acidic properties are partly affected by countercations of silsesquioxane precursors, whereas their pore structures are not influenced much.

The specific novel findings in the present study in light of previous works by us and others [26–36] are the exceptionally high catalytic activities of these oxides for the cracking reactions desite their amorphous nature and the moderate effects of precursor molecules, especially countercations, on the catalytic activities as well as the preparation of new silsesquioxane derivatives, whereas pore structures found in the oxides in this study are in the range reported in the previous papers [26–34]. The surface acidic sites of the oxides discussed here are also found to be stronger than those of usual amorphous aluminosilicates, but slightly lower than those of HZSM-5 zeolites. Our effort is now focused on the enlargement of micropores of the oxides in order to accommodate larger molecules as well as improvement of their acidic properties.

Acknowledgments

A part of this work has been carried out as a research project of the Japan Petroleum Institute commissioned by the Petroleum Energy Center with a subsidy from the Ministry of International Trade and Industry, and supported in part by a Grant-in Aid for Scientific Research (No. 16560676) from the Ministry of Education, Science, Sports, and Culture. The authors are grateful to Dr. S. Iwamoto for his kind instruction regarding TPD measurements.

References

[1] J.G. Speight, The Chemistry and Technology of Petroleum, Dekker, New York, 1991.
[2] K. Weissermel, H.J. Arpe, Industrial Organic Chemistry, VCH, Frankfurt, 1988.
[3] F.J. Feher, T.A. Budzichowski, Polyhedron 14 (1995) 3239.
[4] R.H. Baney, M. Ito, A. Sakakibara, T. Suzuki, Chem. Rev. 95 (1995) 1409.
[5] R. Murugavel, A. Voigt, M.G. Walawalker, H.W. Roesky, Chem. Rev. 96 (1996) 2205.
[6] P.G. Harrison, J. Organomet. Chem. 542 (1997) 141.
[7] H.C.L. Abbenhuis, Chem. Eur. J. 6 (2000) 25.
[8] T. Mitsudo, K. Wada, Shokubai 42 (2000) 282.
[9] V. Lorenz, A. Fischer, S. Giessmann, J.W. Gilje, Y. Gun'ko, K. Yacob, F.T. Edelmann, Coord. Chem. Rev. 206–207 (2000) 321.
[10] R. Duchateau, Chem. Rev. 102 (2002) 3525.
[11] F.J. Feher, T.A. Budzichowski, J.W. Ziller, Inorg. Chem. 36 (1997) 4082.
[12] F.J. Feher, T.A. Budzichowski, J.W. Ziller, J. Am. Chem. Soc. 111 (1989) 7288.
[13] F.J. Feher, J.W. Ziller, Organometallics 9 (1990) 2638.
[14] F.J. Feher, K.J. Weller, J.W. Ziller, J. Am. Chem. Soc. 114 (1992) 9686.
[15] F.T. Edelmann, Y.K. Gun'ko, S. Giessmann, F. Olbrich, Inorg. Chem. 38 (1999) 210.
[16] R. Duchateau, R.J. Harmsen, H.C.L. Abbenhuis, R.A. van Santen, A. Meetsma, S.K.H. Thiele, M. Kranenburg, Chem. Eur. J. 5 (1999) 3130.
[17] M.D. Skowronska-Ptasinska, R. Duchateau, R.A. van Santen, G.P.A. Yap, Eur. J. Inorg. Chem. (2001) 133.
[18] G. Gerritsen, R. Duchateau, R.A. van Santen, G.P.A. Yap, Organometallics 22 (2003) 100.
[19] F.J. Feher, T.A. Budzichowski, J.W. Ziller, Inorg. Chem. 31 (1992) 5100.
[20] R. Duchateau, R.A. van Santen, G.P.A. Yap, Organometallics 19 (2000) 809.
[21] H.C.L. Abbenhuis, H.W.G. van Herwijnen, R.A. van Santen, Chem. Commun. (1996) 1941.
[22] S. Krijnen, H.C.L. Abbenhuis, R.W.J.M. Hanssen, J.H.C. van Hooff, R.A. van Santen, Angew. Chem. Int. Ed. 37 (1998) 356.
[23] S. Krijnen, B.L. Mojet, H.C.L. Abbenhuis, J.H.C. van Hooff, R.A. van Santen, Phys. Chem. Chem. Phys. 1 (1999) 361.
[24] M.D. Skowronska-Ptasinska, M.L.W. Vorstenbosch, R.A. van Santen, H.C.L. Abbenhuis, Angew. Chem. Int. Ed. 41 (2002) 637.
[25] K. Wada, M. Nakashita, A. Yamamoto, H. Wada, T. Mitsudo, Chem. Commun. (1998) 113.
[26] K. Wada, M. Nakashita, M. Bundo, K. Ito, T. Kondo, T. Mitsudo, Chem. Lett. (1998) 659.
[27] K. Wada, M. Bundo, D. Nakabayashi, N. Itayama, T. Kondo, T. Mitsudo, Chem. Lett. (2000) 628.
[28] K. Wada, K. Yamada, T. Kondo, T. Mitsudo, Chem. Lett. (2001) 12.
[29] K. Wada, K. Yamada, T. Kondo, T. Mitsudo, J. Jpn. Petrol. Inst. 45 (2002) 15.
[30] N. Maxim, H.C.L. Abbenhuis, P.J. Stobbelaar, B.L. Mojet, R.A. van Santen, Phys. Chem. Chem. Phys. 1 (1999) 4473.
[31] N. Maxim, H.C.L. Abbenhuis, P.C.M.M. Magusin, R.A. van Santen, Chinese J. Chem. 19 (2001) 30.
[32] N. Maxim, P.C.M.M. Magusin, P.J. Kooyman, J.H.M.C. van Wolput, R.A. van Santen, H.C.L. Abbenhuis, Chem. Mater. 13 (2001) 2958.
[33] N. Maxim, A. Overweg, P.J. Kooyman, J.H.M.C. van Wolput, R.W. J.M. Hanssen, R.A. van Santen, H.C.L. Abbenhuis, J. Phys. Chem. 106 (2002) 2203.
[34] N. Maxim, A. Overweg, P.J. Kooyman, A. Nagy, R.A. van Santen, H.C.L. Abbenhuis, J. Mater. Chem. 12 (2002) 3792.
[35] R. Murugavel, P. Davis, V. Shete, Inorg. Chem. 42 (2003) 4696.
[36] Y. Imizu, K. Takahara, N. Okazaki, H. Itoh, A. Tada, R. Ohnishi, M. Ichikawa, Stud. Surf. Sci. Catal. 90 (1994) 339.
[37] D.D. Perrin, W.L.F. Armarego, Purification of Laboratory Chemicals, third ed., Pergamon, Oxford, 1988.
[38] H.C.L. Abbenhuis, A.D. Burrows, H. Kooijman, M. Lutz, M.T. Palmer, R.A. van Santen, A.L. Spek, Chem. Commun. (1998) 2726.
[39] K. Wada, K. Yamada, D. Izuhara, T. Kondo, T. Mitsudo, Chem. Lett. (2000) 1332.
[40] C.G. Lugmair, K.L. Fujdala, T.D. Tilley, Chem. Mater. 14 (2002) 888.
[41] S.J. Greg, K.S.W. Sing, Adsorption, Surface Area and Porosity, second ed., Academic Press, London, 1982.
[42] A. Saito, H.C. Foley, AIChE J. 37 (1991) 429.

[43] P.A. Agaskar, J. Chem. Soc., Chem. Commun. (1992) 1024.
[44] R.A. Mantz, P.F. Jones, K.P. Chaffee, J.D. Lichtenhan, J.W. Gilman, Chem. Mater. 8 (1996) 1250.
[45] For example, M. Yabuki, R. Takahashi, S. Sato, T. Sodesawa, K. Ogura, Phys. Chem. Chem. Phys. 4 (2002) 4830.
[46] K. Okumura, K. Nishigaki, M. Niwa, Chem. Lett. (1998) 577.
[47] F. Moulder, W.F. Stickle, P.E. Sobol, K.D. Bomben, Handbook of X-Ray Photoelectron Spectroscopy, Perkin–Elmer Co., Eden Prairie, 1992.
[48] Y. Okamoto, H. Tomioka, Y. Katoh, T. Imanaka, S. Teranishi, J. Phys. Chem. 84 (1980) 1833.
[49] K. Wada, K. Yoshida, Y. Watanabe, J. Chem. Soc., Faraday Trans. 91 (1995) 1647.
[50] Y. Imizu, Shokubai 30 (1988) 525.
[51] T. Blasco, M.A. Camblor, J.L.G. Fierro, J. Perez-Pariente, Micropor. Mater. 3 (1994) 259.
[52] For example, T. Takeguchi, K. Yanagisawa, T. Inui, M. Inoue, Appl. Catal. A 192 (2000) 201.